PCCP

Modeling Separation of Lanthanides via Heterogeneous Ligand Binding

Journal:	*Physical Chemistry Chemical Physics*
Manuscript ID	CP-ART-02-2024-000880.R2
Article Type:	Paper
Date Submitted by the Author:	25-Jun-2024
Complete List of Authors:	Leung, Kevin; Sandia National Laboratories, Surface and Interface Science Ilgen, Anastasia ; Sandia National Laboratories, Geochemistry Department

Data included in supp_all.pdf.

Modeling Separation of Lanthanides via Heterogeneous Ligand Binding

Kevin Leung* and Anastasia G. Ilgen

[1] *Geochemistry Department, MS 0750,*

Sandia National Laboratories, Albuquerque,

New Mexico 87185, USA; kleung@sandia.gov

(Dated: June 24, 2024)

Abstract

Individual lanthanide elements have physical/electronic/magnetic properties that make each useful for specific applications. Several of the lanthanides cations (Ln^{3+}) naturally occur together in the same ores. They are notoriously difficult to separate from each other due to their chemical similarity. Predicting the Ln^{3+} differential binding energies ($\Delta\Delta E$) or free energies ($\Delta\Delta G$) at different binding sites, which are key figures of merit for separation applications, will help design of materials with lanthanide selectivity. We apply *ab initio* molecular dynamics (AIMD) simulations and Density Functional Theory (DFT) to calculate $\Delta\Delta G$ for Ln^{3+} coordinated to ligands in water and embedded in metal-organic frameworks (MOFs), and $\Delta\Delta E$ for Ln^{3+} bonded to functionalized silica surfaces, thus circumventing the need for the computational costly absolute binding (free) energies ΔG and ΔE. Perturbative AIMD simulations of water-inundated simulation cells are applied to examine the selectivity of ligands towards adjacent Ln^{3+} in the periodic table. Static DFT calculations with a full Ln^{3+} first coordination shell, while less rigorous, show that all ligands examined with net negative charges are more selective towards the heavier lanthanides than a charge-neutral coordination shell made up of water molecules. Amine groups are predicted to be poor ligands for lanthanide-binding. We also address cooperative ion binding, i.e., using different ligands in concert to enhance lanthanide selectivity.

I. INTRODUCTION

Individual lanthanide (Ln) elements have numerous applications.[1,2] However, lanthanides naturally occur as mixtures of trivalent cations (Ln^{3+}) in their ores. Separating the chemically similar Ln^{3+} from each other is a technologically relevant and chemically challenging problem.[3–7] Much experimental[3,5–13] and theoretical work[14–21] has focused on this separation issue using organic ligands, sometimes in organic solvents. In this work, we investigate the use of simple ligands dissolved in water, or tethered to silica and metal-organic framework interior surfaces in aqueous media, to illustrate fundamental principles that lead to differential Ln^{3+} binding free energies relevant to separation.

For ligands in water, we use simple anions and molecules like sulfate,[22–24] phosphate,[25] and primary amines,[26,27] which have been demonstrated to bind to Ln^{3+}, so there is less concern about desorption during long trajectories. Our work on Ln^{3+}-complexes at infinite dilution in water builds on the extensive computational studies of hydration properties of lanthanides.[28–35] For silica in aqueous media, we choose as ligands, tethered to the surfaces, those used to functionalize MOF interior in recent experiments,[13] because ligands like aspartic acid, with both -OH and amine groups, have been shown to effectively bind to Ln^{3+}.[36] We will show that these simple anionic species exhibit Ln^{3+} binding trends consistent with more complex supermolecules containing N- and O-terminated groups.[20,21] Silica, with and without functionalization of surfaces, have been shown to adsorb[37–39] and to some extent separate[40–42] Ln^{3+} in aqueous media. These aqueous systems present green solvent options, compared with supermolecular macrocycle ligands used in "solvent extraction" which can involve organic solvents/co-solvents,[43] and compared with commercial rare earth extraction where various acids, ketones, esters, and amines may be involved.[44] The role of functionalized material surfaces in aqueous media in rare earth mining has also been reported.[45–47] MOFs, with/without functionalization, have emerged as promising Ln^{3+} separation platforms in aqueous media.[7,9,13] We do not consider functionalization in the MOF interior in this work, but further development of such inorganic materials will likely enhance their Ln^{3+} selectivity, making them competitive with organic materials or macromolecules which are arguably less durable and less environmentally benign.

One theme we will examine is cooperative ion binding using two dissimilar ligands. Cooperative ion adsorption has been recognized as a potent mechanism for separations in biological systems,[48] was explored for molecular recognition,[49–52] for the separation of chemically-

similar species,[53,54] and to design sensors based on ion-selective interactions.[55] Lanthanide ions can complex with organic ligands and then bind selectively to cancerous tumors;[50] similarly lanthanide complexes can be used to detect saccharides in biological fluids.[51] Our understanding of the cooperative binding mechanisms remains elusive because it is the complex function of a favorable combination of two or more molecular forces: van der Waals, dipole-dipole, H-bonding, and electrostatic interactions. Previous work on selected lanthanide ions confined within reverse micelles indicates that cooperative interactions, determined by reverse micelle size, H_2O content, and acidity, lead to changes from mono- to bi-dentate lanthanide coordination with respect to nitrate aqueous ligands.[56] Literature reports discussing cooperative binding of lanthanides in aqueous solutions are scarce, and there are no studies examining these cooperative interactions on material surfaces or water-filled nanopores for the selective capture of lanthanides. We begin to address this fundamental science gap.

Density Functional Theory (DFT) calculations have been conducted for rare earth-organic ligand complexes in aqueous media[14,15,18,57–63] to separate trivalent rare earths from trivalent actinide cations.[16,64–69] Specifically, complexation reactions of Ln^{3+} with EDTA,[58] phosphates and thiophosphates,[63,65] macrocycles,[60] and carboxylic acids have been the subject of DFT studies.[57] These calculations show that separations are determined by the active site donor elemental identity (O, N, S atoms),[57,66] which is related to hard-soft donor property and covalency,[16,58,59,67] to lanthanide ionic sizes and ligand strain/rigidity,[14,60,61,70] counter-anion effects,[14,15,63] to pH and ligand pKa,[69] and to lipophilicity.[64] These descriptor-based methods and analyses[71] can support our choice of the surface groups to be tethered on surfaces or inside MOFs, in addition to investigating cooperative binding effects.

Next we outline the computational methods used, and the challenges we face. Density functional theory (DFT)-based Ln^{3+} and actinide selectivity calculations have been reported extensively in the literature.[14–17,20,21] The vast majority are calculations on isolated, molecular systems (i.e., no periodic boundary conditions, PBC). In these modeling work, the ligands coordinated to the Ln^{3+}, and the first hydration shell of water if present, are depicted explicitly, using DFT configuration-optimization, effectively annealing the ligand-Ln^{3+} binding site to the global energy minimum at T=0 K. The solvation contributions of the media farther away are dealt with using implicit methods.

This approach is not ideal for modeling of ligands anchored to MOF, silica surfaces, or solid state support immersed an aqueous media. Non-PBC codes are not efficient for

periodically replicated simulation cells used for solids. Furthermore, in heterogeneous environments, determining the number of water molecules in the Ln^{3+} first hydration shell, and the extent of hydrolysis events (formation of OH^-) therein, are more suited for DFT-based *ab initio* molecular dynamics (AIMD) simulations in an explicit water-filled PBC simulation cell such that the first hydration shell can exchange water with the aqueous environment. Indeed, Ln^{3+} coordination in pure water has been reported with AIMD simulations.[73,74] AIMD plus potential-of-mean-force (PMF) (including modern metadynamics variants) is a rigorous approach to calculate ion desorption free energies.[74–77] AIMD also permits the modeling of spontaneous proton transfer, including hydrolysis in the Ln^{3+} first hydration shell that can accompany ion adsorption/desorption.

Unfortunately, AIMD-PMF is computationally costly. Long (>20 ps) trajectories are typically required for each stage of PMF. Perturbative approaches where a Ln^{3+} is "alchemically" switched for a neighboring Ln^{3+} should be more efficient.[78] To our knowledge, such cation-switching, which should be most productive for chemically similar Ln^{3+}'s next to each other, and are among the most difficult to physically separate, has not been implemented within AIMD simulations. This approach will be demonstrated in ligands-in-water differential binding free energies $\Delta\Delta G$ calculations herein.

Even perturbative AIMD calculations require long trajectories, and are limited to comparing Ln^{3+} in close proximity in the periodic table. A convenient but approximate approach is to use geometry optimization, non-PBC like in molecular calculations. There are multiple issues which make this approach less-than-rigorous. (1) The PBC-based DFT software used for material systems typically lack molecular-fragment-based optimization tools that enable an efficient search of the global energy minimum (electronic supporting information, ESI, Fig. S2). (2) With more than one hydration shell and a solid substrate present, finding the global minimum may not be relevant even with the best configuration optimization tools. Such local minima results would not be reproducible by other researchers even in principle, as illustrated in ESI section S2. Consider the simplest case of a single Ln^{3+} in a periodically replicated simulation cell containing liquid water with its three-dimensional hydrogen bond network. Most optimization modules in PBC-DFT codes, which track the forces and motion of each atom instead of molecular fragments, will yield glassy ice. Such local minima results would not be reproducible by other researchers even in principle. This may be all the more true when a solid substrate, which strongly binds to water molecules, is present. Even if the

global minimum is successfully predicted, we would have obtained ice I_h, not liquid water – also the incorrect answer for aqueous media.

In this work, we pursue an approach that makes no claim for complete rigor, but is expected to yield insight for the sole purpose of calculating the relative binding energies ($\Delta\Delta E$) of 14 Ln^{3+} from Ce^{3+} to Lu^{3+}. (1) We first conduct short AIMD trajectories with an explicit liquid water environment that predict key structural properties (e.g., number of water molecules in the first hydration shell of Ln^{3+} already bound to 2 ligands, and the extent of water hydrolysis). (2) We eliminate all water molecules not in the Ln^{3+} first hydration shell, except a few bound to obviously negatively charged ligand atoms on substrate surfaces, and perform configuration optimization. Simulated annealing is also considered but does not improve the results. (3) Finally, we replace the Ln^{3+} with one of the other 13 Ln^{3+} in the series, usually a neighbor in the periodic table, and re-optimize. (4) We compare with results for pure water in the Ln^{3+} first hydration shell. See the "Method" section for details. The relative energies obtained from these representative local minimum configurations are valuable in determining whether certain combinations of ligands participate in cooperative binding, becoming more favorable to either heavier or lighter lanthanides.

II. METHOD

DFT calculations are conducted with the Perdew-Burke-Ernzerhof (PBE) functional,[81] the Vienna Atomic Simulation Package (VASP),[82–85] a 400 eV energy cutoff, and Γ-point sampling of the Brillouin zone. For static DFT calculations, a Born-Oppenheimer energy convergence criterion of 10^{-4} eV is enforced. For AIMD simulations, the criterion is 10^{-6} eV, the time step is 0.5 fs, and the temperature is set at T=400 K using a Nose thermostat. In all cases, dispersion correction, such as DFT-D3,[86] is not included.[87]

The VASP lanthanide projected augmented wave pseudopotential used are those with $4f$ electrons subsumed into the pseudocore: "Ce 3 06Sep2000," "Pr 3 07Sep2000," "Nd 3 06Sep2000," "Pm 3 07Sep2000," "Sm 3 07Sep2000," "Eu 3 20Oct2008," "Gd 3 06Sep2000," "Tb 3 06Sep2000," "Dy 3 06Sep2000," "Ho 3 06Sep2000," "Er 3 06Sep2000," "Tm 3 20Jan2003," "Yb 3 08Jul2013," and "Lu 23Dec2003." Some comparisons of these pseudopotentials and the PBE functional with quantum chemistry approaches have been made.[74] Our main goal in this work is not to generate the most accurate *ab initio* results possible, but to present Ln^{3+} binding energy trends based on a compromise of accuracy and computational

efficiency.

AIMD simulations include: Ln^{3+} plus two ligand molecules/ions in liquid water, Ln^{3+} in a MOF filled with water, and Ln^{3+} adsorbed on functionalized silica surfaces in contact with liquid water. In the first two cases, the objective is to calculate the change in free energy ($\Delta\Delta G$) when a Ln^{3+} is substituted for another Ln^{3+} at a binding site. Normally this requires calculating adsorption/desorption free energies for both Ln^{3+}. AIMD desorption free energy calculations generally involve costly PMF calculations and a bulk-water-like reservoir region, which mandates a sizable simulation cell.[74] Instead we estimate $\Delta\Delta G$ using first order perturbation theory within an equilibrium ensemble, which has been implemented using classical force fields[78] but to our knowledge not AIMD:

$$\Delta\Delta G_{\mathrm{b,a}} \approx \langle \Delta E_{\mathrm{b}} - \Delta E_{\mathrm{a}} \rangle_{\mathrm{a}}. \quad (1)$$

Here $\langle\rangle_{\mathrm{a}}$ refers to averages generated using an AIMD trajectory with the "a" Ln^{3+} pseudopotential, and ΔE_{x} is the energy difference between a liquid state configuration with a Ln^{3+} and that Ln^{3+} in the gas phase. $\Delta\Delta G$ is sampled every 100 AIMD time steps. The reference free energy is the first ("a") Ln^{3+} in these perturbative simulations. For added confirmation, we run the averages with both the "a" and "b" pseudopotentials, and average the results. Generating trajectories using both pseudopotentials and averaging eliminates the second order perturbation; the highest order error of the method would then be the third order term in pseudopotential difference. Both homogeneous (two identical ligands) and cooperative (two dissimilar ligands) cases are considered. Ideally, one would calculate $\Delta\Delta G$ for all neighbors among the 14 lanthanides under consideration, but AIMD simulations remain costly, even when performed in this perturbative mode. Hence we only consider the Dy^{3+}/Tb^{3+} pair. This serves as a proof-of-principle calculation for a technique that will be called upon for future, accurate $\Delta\Delta G$ calculations of Ln^{3+}-selective binding sites found promising by other pre-screening computational techniques. The translational entropy term, due to deviation from the computational standard (1.0M concentration) should cancel when comparing one Ln^{3+} with another.

Most of the bulk-water-like AIMD simulation cells are charge-neutral, have dimensions 18×12×12 $Å^3$, and contain one Ln^{3+}, two ligands, and 85 H_2O molecules. The ligand pairs include SO_4^{2-}/HSO_4^-, $H_2PO_4^-/HPO_4^{2-}$, $H_2PO_4^-/SO_4^{2-}$, and $(NH_2)_2C_2H_4/PO_4^{3-}$. As will be shown, the diamine-lanthanide motif can transform into R-NH_3^+-OH^--Ln^{3+}. PMF approach to calculate the free energy associated with this change with a 24×12×12 $Å^3$ with 114 H_2O

molecules. Here the Ln^{3+} and the N atom of the NH_2 group initially attached to it are frozen in the x- and y-directions with the same x- and y-coordinates; their relative displacement (R) in the z-direction is controlled by harmonic potentials of the form $V(R) = A(R - R_o)$. The parameters and other details are given in the ESI Sec. S4.

We also consider single Ln^{3+} in (12.42 Å)^3 simulation cells with 64 H_2O molecules; such simulation cells have $+3|e|$ net charges, where $|e|$ is the electronic charge. Normally the well-known monopole correction is needed to correct the absolute hydration free energies of charged ions in water in charged simulation cells.[88] This correction should largely cancel for the difference in free energies with two similarly charged cations. Our $\Delta\Delta G$ calculations for Ln^{3+} assumes non-interacting periodic image, which amounts to assuming Ln^{3+} are at infinite dilution.

The numbers of H_2O molecules in all AIMD simulation cells are determined as follows. Classical force field-based grand canonical Monte Carlo (GCMC)[89] simulations are first applied to determine the average number of water molecules in the cell.[90] The SPC/E water model,[91] the ClayFF a force field for silica[92] if present, and generic force field parameters pertinent to Ln^{3+} are adopted for this purpose. Substrate atoms, ligands (if present), and the adsorbed cation are frozen in water-free, DFT-optimized positions in GCMC calculations; only water molecules are inserted into or removed from the simulation cell, and are allowed to translate and rotate therein. The number of H_2O molecules coordinated to the Ln^{3+} depends on the surfaces and the ligands (phosphates, sulfates, and primary amines) dispersed in water. From the last GCMC configurations, AIMD simulations are initiated.

In static calculations, we define the absolute Ln^{3+} adsorption or binding energy (ΔE) as

$$\Delta E = E_{\rm tot} - E_{\rm substrate} - E_{\rm Ln^{3+}}, \tag{2}$$

where $E_{\rm Ln^{3+}}$ is the energy of a Ln^{3+} cation by itself in a simulation cell, $E_{\rm tot}$ is the total energy of the optimized simulation cell with the Ln^{3+} coordinated to the substrate at the binding site, and $E_{\rm substrate}$ is the energy of the substrate in the absence of the Ln^{3+}. The substrate may be the first hydration shell, or an entire silica slab. If the simulation cell for $E_{\rm tot}$ is charge neutral, $E_{\rm substrate}$ would be the energy of system with a net $-3|e|$ charge, where $|e|$ is the electronic charge. It would have been difficult to calculate correctly because a monopole correction would have to be applied in a spatially inhomogeneous system.

Fortunately we never need to report ΔE in this work. Instead, we define the differential binding energy $\Delta\Delta E$ as the ΔE of a Ln^{3+} ("Ln_b") relative to another Ln^{3+} ("Ln_a," typically

Ce), via

$$\Delta\Delta E = \Delta E_{\mathrm{Ln}_b} - \Delta E_{\mathrm{Ln}_a}. \quad (3)$$

$E_{\mathrm{substrate}}$ cancels out. $E_{\mathrm{Ln}^{3+}}$ should include a monopole correction, which in our case is not strictly necessary, because it should be similar for the different Ln^{3+}, and should cancel in $\Delta\Delta E$.

Likewise, in AIMD simulations, we never calculate ΔG of Ln^{3+} in aqueous media with ligands. Calculating such ΔG would be similar to computing the absolute hydration free energies of ions in water using AIMD thermodynamic integration (TI).[93,94] These are increasingly computatioally difficult with increasing cation charges because more TI integration points would be needed to account for the rapid change in hydration structure as the local charge density increass; such calculations would constitute separate research projects and are not within the scope of this work. Calculating the absolute binding free energy in nanoporous materials, like UiO-66 in our case, via AIMD potential-of-mean-force techniques,[75] is also problematic because AIMD simulation nanopore simulation cells seldom contain a bulk water reservoir region needed to yield the proper reference state for standard state binding free energies.

$\Delta\Delta\Delta E$ is the difference between $\Delta\Delta E$ for a particular substrate and that with a 8-H_2O hydration shell.

$\Delta\Delta E$ of the lanthanide series adsorbed on functionalized silica surfaces, referenced to Ce^{3+} binding energies, are examined using an approximate procedure less costly than AIMD perturbation, as follows. First AIMD is used for equilibration of the first hydration shell of Ln^{3+} bound to ligands and/or substrate surface sites in a water-filled simulation cell. While the Ln^{3+} coordination numbers in liquid water at neutral pH are well-documented,[29] they are less well known in the presence of ligands, surface binding sites, and anions[32] like possible OH^- from the hydrolysis of H_2O which can be rapidly equilibrated in AIMD trajectories. As a non-lanthanide example, Al^{3+} is known to be 6-coordinated at low pH but 4-coordinated at high pH due to repulsion between the OH^- species bound to the Al cation.[95,96] After AIMD equilibration for 4.0 ps, most H_2O molecules are removed except those coordinated to the Ln^{3+} and those coordinated to formally negatively charged groups of ligands which are not themselves coordinated to the Ln^{3+} or the substrate surface.

Optimization of the resulting atomic configuration is then carried out, quenching the structure to T=0 K. $\Delta\Delta E$'s for Ln^{3+} are obtained by sequentially substituting the Ln^{3+}

pseudopotentials by that of a neighboring one in the periodic table and calculating the energy difference between each Ln^{3+} and that of Ce^{3+}, after subtracting the isolated Ln^{3+} gas phase ion energy. Both Ce^{3+} and Lu^{3+}, which bracket the Ln^{3+} considered herein, are used to generate AIMD-equilibrated configurations and initiate the above procedure. $\Delta\Delta E$ for these two options should be equal if the systems have reached the global minima. Instead, we have found that one round of optimization yields $\Delta\Delta E$ that can differ by >1 eV depending on whether Ce^{3+} or Lu^{3+} AIMD is applied. The reason is that the system can get trapped in metastable structures. Instead, we repeatedly do the following; for Ce-generated AIMD we go down the series from Ce the series to Lu and then up again, with each optimization starting from previous Ln^{3+}'s configuration, until $\Delta\Delta E$ between Ce and Lu converges to within 0.05 eV. For Lu-generated AIMD, we similarly go up from Lu to Ce and down again, until $\Delta\Delta E$ between Ce and Lu converges to within 0.05 eV. This is an empirical solution; improvement in the method will be considered in the future.

The base simulation cells with β-cristobalite (110) silica substrate have dimensions $20.25\times14.32\times26$ Å^3, with a stoichiometry of $Si_{80}O_{186}H_{32}$. The SiOH surface density is about 5 nm^{-2}. The tethered organic ligands include 1H-pyrazole-4-carboxylic acid (henceforth PYC), aminotri(methylenephosphonic acid) (henceforth NP_3), oxalate, and aspartic acid. As mentioned above, these ligands are selected because they have been used to functionalize MOFs for Ln^{3+} separation purposes,[13] and some have been demonstrated to bind effectively to Ln^{3+}.[36] Two ligands, not necessarily of the same type, are grafted on to β-cristobalite (110) surfaces, with their anchoring groups replacing two surface OH groups while polar or negatively charged terminals are oriented to coordinate to Ln^{3+}. Three H^+ are removed from either SiOH groups nearby or one of the H_2O also coordinated to the absorbed Ln^{3+} during equilibration. In most cases, the two neighboring SiOH anchoring sites are selected at random. For one ligand (PYC), two distances between the anchoring sites are considered. We stress that these simulation cells are meant to be model system; experimental realizations of such tethered ligands, especially chemically heterogeneous ligands, have not been reported. The results should be pH-dependent; at high pH values, lanthanides are less soluble and precipitate as hydroxides.[97] This work focuses on near pH-of-zero-charge conditions.

We are mostly concerned with selective adsorption and separation of lanthanides, which are related to relative binding (free) energies. However, Ln^{3+} must have higher absolute

binding free energies (ΔG) at the binding sites than hydration free energies in water for the separation material. If the binding sites are weak and only a low percentage of Ln^{3+} adsorbs, most Ln^{3+} remain in the water phase and the material would be inefficient for separation. Absolute adsorption free energies (ΔG) are however difficult to calculate using AIMD. In static DFT calculations in periodically replicated simulation cells and material substrates, the system will almost inevitably be trapped in metastable configurations. Furthermore, ΔE of a charged species (Ln^{3+}) within a charge-neutral, periodically replicated, spatially inhomogeneous simulation cell is not well defined.[93] Fortunately, whether a certain Ln^{3+} binds to a substrate can be determined experimentally. Based on available experimental data,[13,22–27] we assume that sufficent ligand-Ln^{3+} binding is achieved in all cases, except for amines discussed in the Results Section. Post-adsorption treatment, like flushing to desorb Ln^{3+}, is beyond the scope of this work.

The UiO-66 simulation cell has dimensions $20.95\times20.95\times20.95$ Å^3 and a $Zr_{24}C_{192}O_{128}H_{112}$ stoichiometry. GCMC simulations determine that 130 H_2O water molecules reside in this MOF simulation cell. The Ln^{3+} is coordinated to a deprotonated O^{2-} anion in the $Zr_6O_8H_n$ cluster of the MOF structure.

III. RESULTS

A. Ln^{3+} in water with ligands

Fig. 1 depicts snapshots of various ligands bound to Dy^{3+} in water. Trajectories generated using Dy^{3+} and Tb^{3+}, adjacent to each other in the periodic table, generally yield similar configurations. The coordination numbers in the six panels are determined by a Ln^{3+}-O or Ln^{3+}-N cutoff distance of 3.2 Å, which is approximately the first minimum in the Ln-O pair correlation function ($g(r)$) in water in our AIMD simulations (ESI Fig. S4). They are all 7-coordinated in these snapshots except for Fig. 1f which has a 6-coordinated Dy^{3+}, and are less than the 8 to 9-coordinated typically reported for Ln^{3+} in water.[29] For averages over the trajectories, see Table I. The lower coordination numbers are partly due to the anions in the first hydration shell which repel other partially negatively charged species, and partly due to the use of the PBE functional which slightly underestimates even Ln^{3+}-water coordination, yielding 7.3-7.4 instead of 8 for Dy^{3+} and Tb^{3+} in liquid water.

Sec. S1 of the electronic supporting information (ESI) shows that adding the D3 cor-

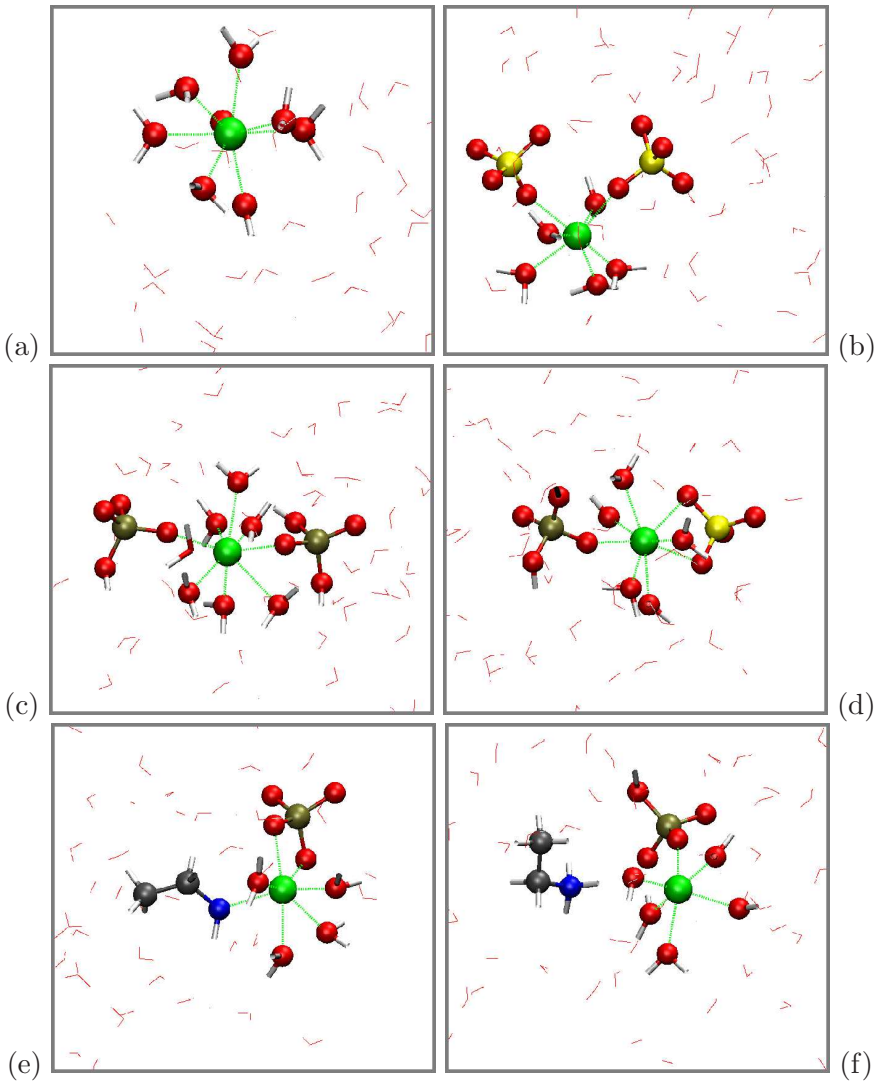

FIG. 1: Snapshots of ligands considered in AIMD $\Delta\Delta G$ simulations. (a) Water; (b) SO_4^{2-}/HSO_4^{-}; (c) $HPO_4^{2-}/H_2PO_4^{-}$; (d) $SO_4^{2-}/H_2PO_4^{-}$; (e)-(f) $CH_3CH_2NH_2/PO_4^{3-}$ initial and final configurations in PMF simulations. Grey, red, blue, white, yellow, dark green, and light green spheres represent C, O, N, H, S, P, and Ln^{3+}. Green dashed lines depict Ln^{3+}-O or Ln^{3+}-N coordination. Stick figures are H_2O molecules not in the first hydration shell. In panel (b), both SO_4^{2-} coordinated to the Ln^{3+} are completely deprotonated; a H_3O^{+} exists elsewhere in the cell to compensate for the negative charge.

rection to static PBE calculations lead to small changes in forces and relaxations in PBE-optimized atomic configurations. However, we acknowledge that AIMD simulations sample configurations away from near-zero-force regions of configuration space. A re-examination of dispersion force effects on CN will be considered in the future.[87]

system	CN	system	CN
Dy^{3+}	7.3	Tb^{3+}	7.4
Dy^{3+}, $HPO_4^{2-}/H_2PO_4^-$	7.1	Tb^{3+}, $HPO_4^{2-}/H_2PO_4^-$	7.3
Dy^{3+}, $SO_4^{2-}/H_2PO_4^-$	7.2	Tb^{3+}, $SO_4^{2-}/H_2PO_4^-$	7.5
Dy^{3+}, SO_4^{2-}/HSO_4^-	7.3	Tb^{3+}, SO_4^{2-}/HSO_4^-	7.8

TABLE I: Average coordination number (CN) in AIMD trajectory lengths. All are conducted in liquid water.

Upon switching from Tb^{3+} to Dy^{3+} and using the perturbative approach of Eq. 1, $\Delta\Delta G$ is found to be -0.30 eV to -0.31 eV for all ligands except the amine ($C_2H_5NH_2$) discussed below. The SO_4^{2-}/PO_4^{3-} pair does not cooperatively yield $\Delta\Delta G$ which are significantly different than the homogeneous anion calculations. The same quantity in pure water is -0.29 eV. Although the change is small (0.01 to 0.02 eV), it is a substantial part of thermal energy at T=300 K, and the preference for Dy^{3+} should be readily detectable in measurements, assuming the cancellation in DFT uncertainties in the AIMD correlated sampling calculations is sufficient. This appears to suggest that negatively charged ligands yield more negative $\Delta\Delta G$ going down the periodic table of lanthanides with heavier and smaller cations. This trend, across 14 Ln^{3+} cations, is more fully examined and clearly revealed in later sections.

The most intriguing case is the primary amine, where the possibility of water hydrolysis, turning the $C_2H_5NH_2$ (Fig. 1e) into a $C_2H_5NH_3^+/OH^-$ pair (Fig. 1f), exists. We illustrate this case using Lu^{3+}. The negatively charged OH^- intervening between the NH_3^+ group and the Lu^{3+} cation can then form a favorable adduct between them. We conduct a PMF calculation (Fig. 2) to confirm that the free energy of the outer shell complex mediated by OH^-, at R$\sim$4 Å, is more favorable than the inner shell complex by 0.38 eV. Unfortunately, further displacement of the Dy^{3+} away from the N-atom of the primary amine exhibits almost no free energy penalty or kinetic barrier. This suggests the Ln^{3+} can freely diffuse away without free energy penalties, and that primary amines are weak ligands towards Ln^{3+}, even after hydrolysis of an intervening water molecule to yield an OH^- adduct.

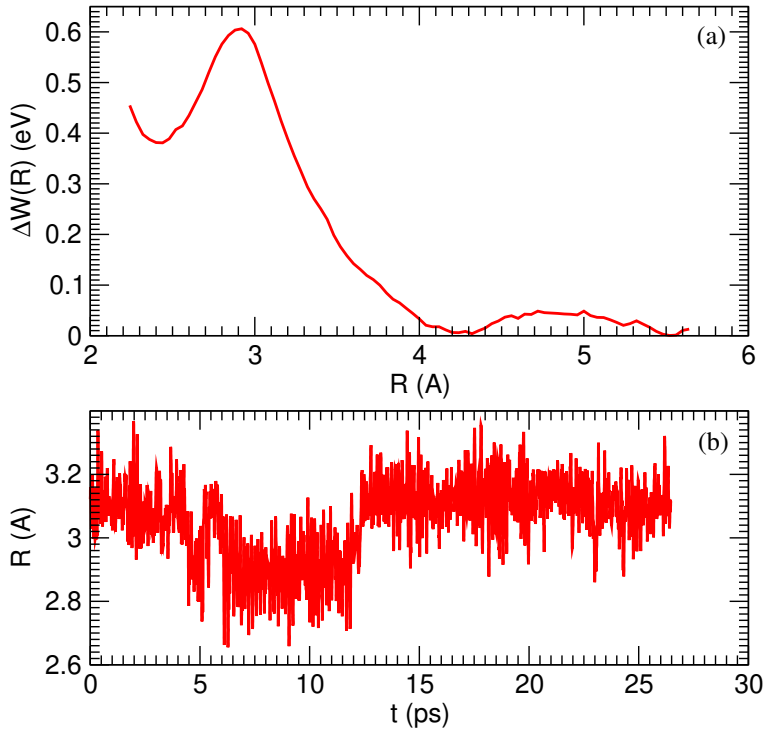

FIG. 2: (a) $\Delta W(R)$ for transforming the $CH_3CH_2NH_2$-Lu^{3+} configuration from inner shell to outer shell with OH^- adduct, and beyond (i.e., Lu^{3+} desorption from the amine). The reaction coordinate R is the distance between the N atom and the Lu^{3+} cation. (b) Time dependences of R near the barrier region as time varies.

B. Ln^{3+} in UiO-66

Fig. 3 depicts an AIMD snapshot of Dy^{3+} at the Zr_4O_6 binding site of a water-filled UiO-66 MOF simulation cell. $\Delta\Delta G$ between Dy^{3+} and Tb^{3+} is once again -0.31 eV, similar to the phosphates, sulfates, and mixed phosphate/sulfate ligands above. This suggests that UiO-66 selectively adsorbs Dy^{3+} over Tb^{3+} by a factor of $\sim$2 from an ionic mixture in water, where the $\Delta\Delta G$ is a smaller -0.29 eV. We stress that this conclusion relies on the assumption that DFT uncertainties can largely cancelled in our correlated sampling perturbative AIMD simulations. The average coordination numbers are 7.9 and 7.9, respectively, when we use a Ln^{3+}-O cut-off distance of 3.25 Å criterion, similar to the case in liquid water. These numbers include 1.0 water molecules and 6.9 O-atoms in the MOF. However, this may be slightly misleading because the distances between the Ln^{3+} and two O-atoms on one linker unit are somewhat larger. Reducing the cut-off distance to 2.90 Å yields coordination numbers 5.9 and 5.8 instead, with the Ln^{3+} coordinated to 1.0 H_2O molecule in each case. In contrast, reducing the cut-off distance in Fig. 1b from 3.25 Å to 2.90 Å only reduces the predicted coordination number by 0.3 %.

The cost of the above AIMD $\Delta\Delta G$ simulations remains substantial. To obtain trends across the selected 14 lanthanide, instead of just neighboring Ln^{3+} in the periodic table, we switch to a more approximate approach in the next section.

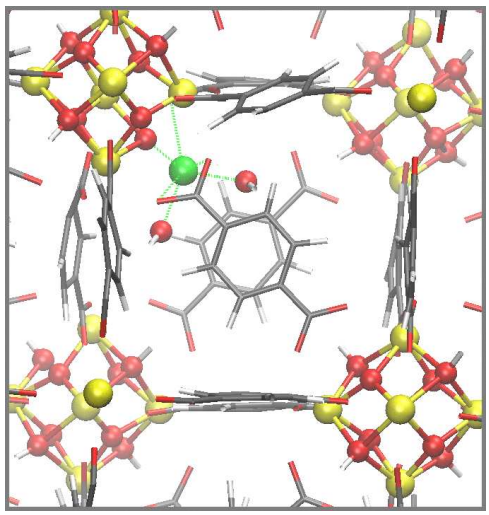

FIG. 3: AIMD snapshot of Dy^{3+} coordinated to a UiO-66 binding site, consisting of two Dy^{3+}-O bonds with the O-anions in the Zr_6O_8 cluster, two Dy^{3+}-O(water) bonds, and two Dy^{3+}-O(linker) bonds. For color key, see Fig. 1. In addition, Zr is depicted as yellow spheres. For easier visualization, water molecules not coordinated to Dy^{3+} are omitted.

C. Simple Clusters: DFT $\Delta\Delta E$

As outlined in the Method Section, we optimize the first coordination shell of either Lu^{3+} or Ce^{3+}, including water and ligands coordinated to silica surfaces. One Ln^{3+} is sequentially substituted for the next heavier or lighter Ln^{3+} in the series (Fig. 4). This is similar to non-PBC-DFT-based calculations for lanthanides in bulk solvents,[14–21] with a few main differences. (1) We omit the implicit solvent, the effect of which should be similar for all lanthanides. (2) Periodic DFT codes, like VASP used herein, are more suited for material substrates. (3) Periodic DFT codes do not have the atom-group configuration sampling feature and will almost certainly be trapped in local minima, as discussed in the Introduction and ESI Sec. S2. We improve the calculations by repeatedly "cycling" through the 14 lanthanides under consideration, moving from Ce^{3+} to Lu^{3+} and back, until the $\Delta\Delta E$ between these two end members converge to 0.05 eV (Method Section). Despite that, our results should be regarded as semi-quantitative.

As a reference system, we calculate $\Delta\Delta E$ of the Ln^{3+} series in a first coordination shell made up of 8 H_2O molecules (Fig. 4). Because of the lack of cross-linking hydrogen bonds, there is much less ambiguity in obtaining the global energy minimum associated with this cluster. The smallest Lu^{3+} exhibits a differential binding energy ($\Delta\Delta E$) with the 8 H_2O molecules which exceeds that of Ce^{3+} by 4.04 eV (Fig. 4a). The $\Delta\Delta E$ magnitude is monotonic across the lanthanide series. Judging from the mean AIMD coordination numbers of ∼7.3-7.4 for Dy^{3+} and Tb^{3+} discussed above, the DFT/PBE functional used herein likely underestimates coordination numbers;[29] therefore we have not considered 9-coordinated Ln^{3+} in clusters with 9 water molecules (ESI Sec. S3).

The 14 Ln^{3+} cations under consideration differ by their number of $4f$ electrons which do not however strongly interact with the environment. To a first approximation, assuming no specific covalent interactions, we expect that negatively-charged ligands will interact more favorably with the heavier and smaller Ln^{3+} compared with uncharged ligands. In other words, $\Delta\Delta E$ (Eq. 1, Fig. 5) should have a steeper slope with negatively charged ligands. The previous AIMD $\Delta\Delta G$ calculations (Figure 1) have already hinted at this effect. Fig. 5a confirms this trend using the simplest of negatively charged ligands: a first coordination shell of 7 H_2O and a OH^- (Fig. 4b), created by randomly removing a H^+ from the Fig. 4a system. $\Delta\Delta E$ for Lu^{3+} is indeed up to 0.35 eV more negative than those for 8 H_2O, with a steeper slope. Fig. 5b emphasizes this point. This fundamental principle for selectivity,

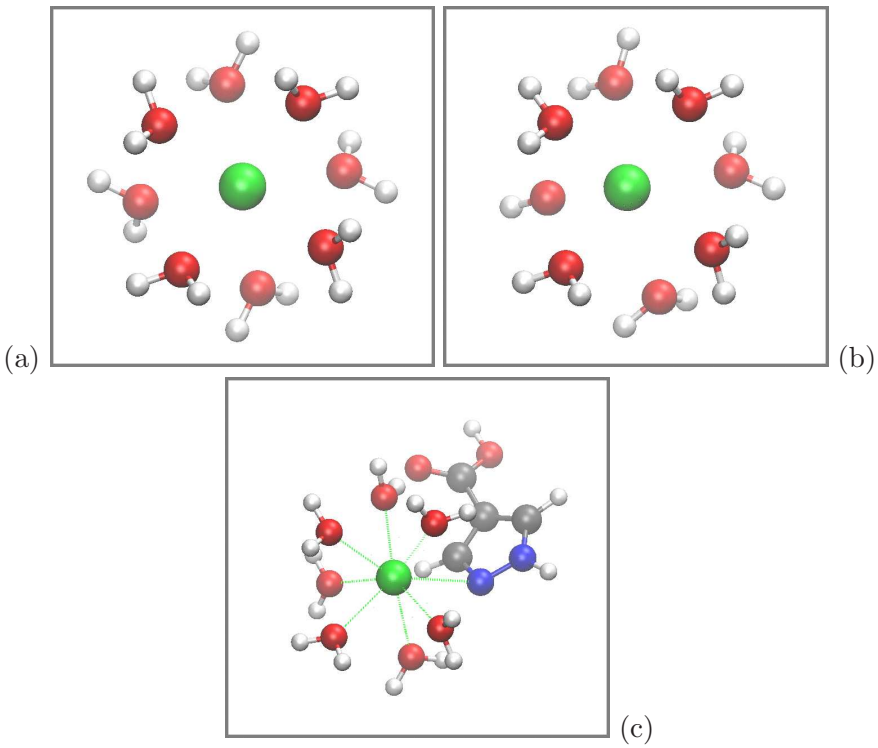

FIG. 4: Optimized (a) $Ln^{3+}(H_2O)_8$, (b) $Ln^{3+}(H_2O)_7OH^-$, and (c) $Ln^{3+}(H_2O)_6PYC$ configurations.

favoring heavier Ln^{3+}, will be revisited in the next section.

Fig. 4c depicts the replacement of OH^- by a PYC ligand via the N-terminus, with the unprotonated N-atom coordinating to the Ln^{3+}, Fig. 5a shows that the $\Delta\Delta E$ slope for PYC plus 7 H_2O is slightly smaller than that for 8 H_2O. This suggests that PYC is a weaker ligand than either H_2O or OH^-, although the magnitude of the change due to PYC is significantly less than that of OH^-. It also suggests that a combination of ligands more attracted to Ln^{3+} than water (e.g., OH^-) and ligands less so attracted (e.g., PYC) might lead to selective capture of lighter Ln^{3+} in the series – provided that the binding site remains overall favored over liquid water despite the addition of one ligand that is weaker than H_2O. We will examine this hypothesis below.

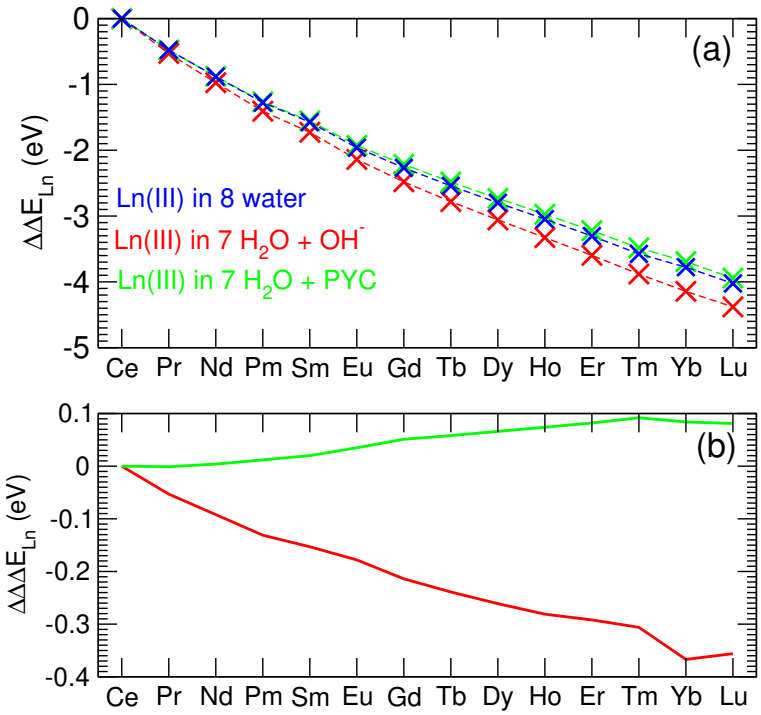

FIG. 5: (a) $\Delta\Delta E$ associated with 8 H_2O (blue), 7 H_2O/OH^- (red), and 7 H_2O/PYC (green) coordinated to Ln^{3+}. (b) Difference between the OH^- and H_2O curves (red), and that between PYC and H_2O (green), are plotted as $\Delta\Delta\Delta E$.

D. Ln^{3+} at Binding Sites on Silica Surfaces

Armed with this insight, we next consider functionalized β-crystobalite surfaces. Figs. 6a-f depict the configurations of Ln^{3+} coordinated to 6 binding sites, with some SiOH groups deprotonated to maintain charge-neutrality. Panels (a) and (b) depict two aspartates with different distances between the aspartate anchors. The coordination number is 7 in both cases. Recall that we start from the Ce^{3+}/Lu^{3+} configurations and sequentially replace the Ln^{3+} with the next heavier/lighter ones. The perturbation in each replacement step is sufficiently small that the coordination numbers and similar atomic configurations are largely conserved. Also note that we use the carboxylate end of the aspartate ligands at the binding site, since -NH_2 groups have previously been shown to bind weakly to Ln^{3+} (Fig. 3). All other binding sites (Fig. 6c-f) exhibit a smaller coordination number of 6 with respect to Ce^{3+}. Since the PYC is anchored to the surface via its carboxylate group (Fig. 6d), by necessity its aromatic nitrogen atom binds to the Ce^{3+}, although this nitrogen is not expected to be a strong ligand (Fig. 5).

Figs. 7a-f depict $\Delta\Delta E$ relative to Ce^{3+} binding for each binding site, and compare that with $\Delta\Delta E$ computed in clusters with 8 water molecules (Fig. 4a). $\Delta\Delta E$ monotonically increases in magnitude going down the series towards smaller, heavier Ln^{3+}. With the "up and down" cycles of optimizing from Ce^{3+} to Lu^{3+} and then back until 0.05 eV convergence is obtained, the $\Delta\Delta E$ series starting from Ce^{3+} and Lu^{3+} AIMD snapshots agree to at least 0.5 eV. They generally agree much better than that. The binding site with the most disagreement occurs for one of the two aspartates configurations. There the Lu^{3+} trajectory series (Fig. 6a) has a water molecule intervening between the Ln^{3+} and a surface SiOH group, while the Ce^{3+} series (not shown) has the Ln^{3+} directly coordinated to a surface SiOH. As water is likely a stronger ligand than SiOH, the difference is reasonable. If we do not conduct the "up and down" iterations, the $\Delta\Delta E$ difference between Ce^{3+}- and Lu^{3+}-AIMD snapshots can differ by more than 1 eV, and it is always the Ce^{3+} trajectory $\Delta\Delta E$, rather than the Lu^{3+} one, which has a larger magnitude.

The slopes with respect to atomic mass are steeper than that for 8-H_2O molecules in all cases in Fig. 7. Thus the binding sites monotonically favor the smaller, heavier Ln^{3+}. As all the sites have at least one negatively charged ligand, including SiO^-, this is consistent with our expectation that negatively charged ligands interact more strongly with heavier Ln^{3+} with small radii than lighter Ln^{3+} with larger radii relative to an uncharged water

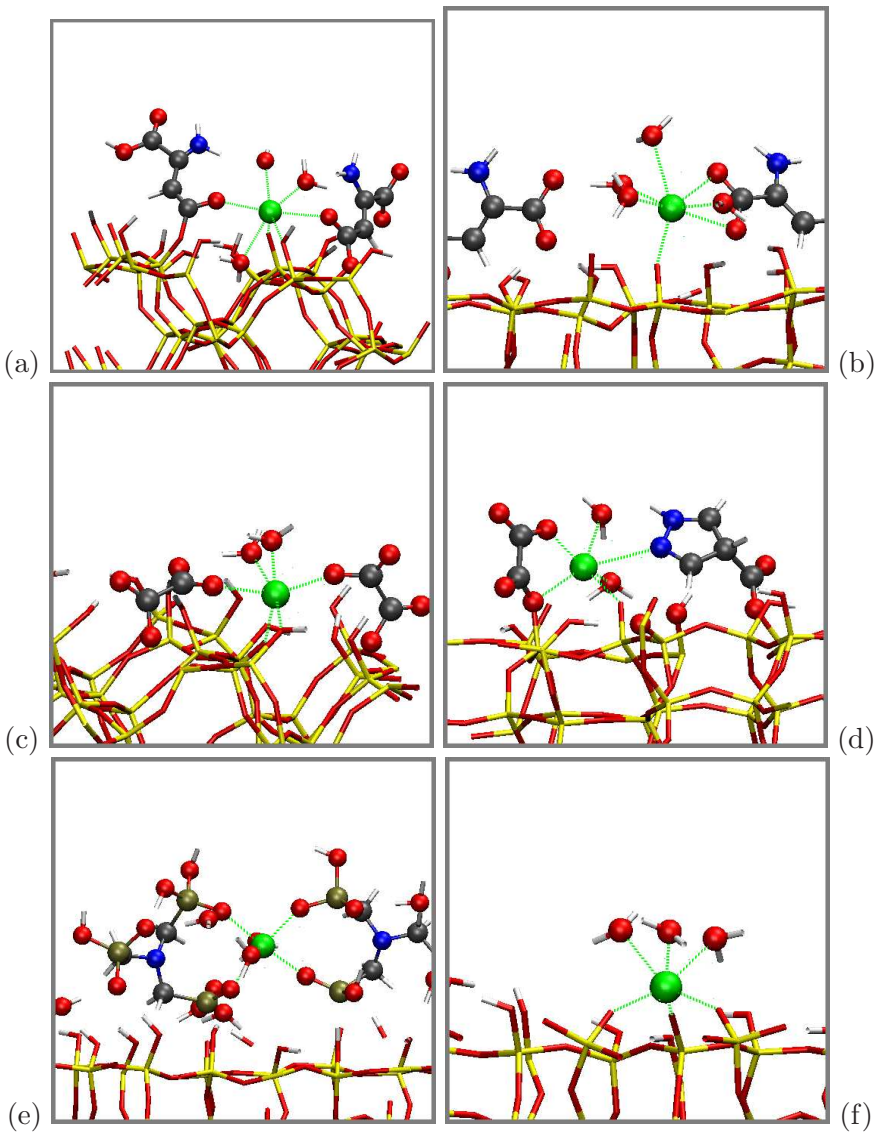

FIG. 6: Lu^{3+} bound to ligands tethered to β-cristobalite surfaces. (a)-(b) 2 aspartates at two different distances; (c) 2 oxalates, (d) oxalate plus PYC; (e) 2 NP_3; (f) bare β-cristobalite with three deprotonated SiOH groups. Grey, red, blue, white, yellow, and green spheres represent C, O, N, H, Si, and Ln^{3+} respectively. Configurations generated by the Ce^{3+} trajectory, not shown, are not identical.

coordination shell (Fig. 4). We further subtract the $\Delta\Delta E$ associated with the ligands from that in water for the 14 Ln^{3+} being considered, and denote the quantity $\Delta\Delta\Delta E$ (Fig. 8). The ligands differentially favor Lu^{3+} over Ce^{3+} by up to 1.1 eV over water. This is qualitatively consistent with the $Ln^{3+}(H_2O)_8$ vs. $Ln^{3+}(H_2O)_7OH^-$ comparison (Fig. 5a-b), except that the magnitude is larger here because the ligands have more negative charges (up to -3$|e|$ formal charges for the bare β-cristobalite surface, Fig. 8f).

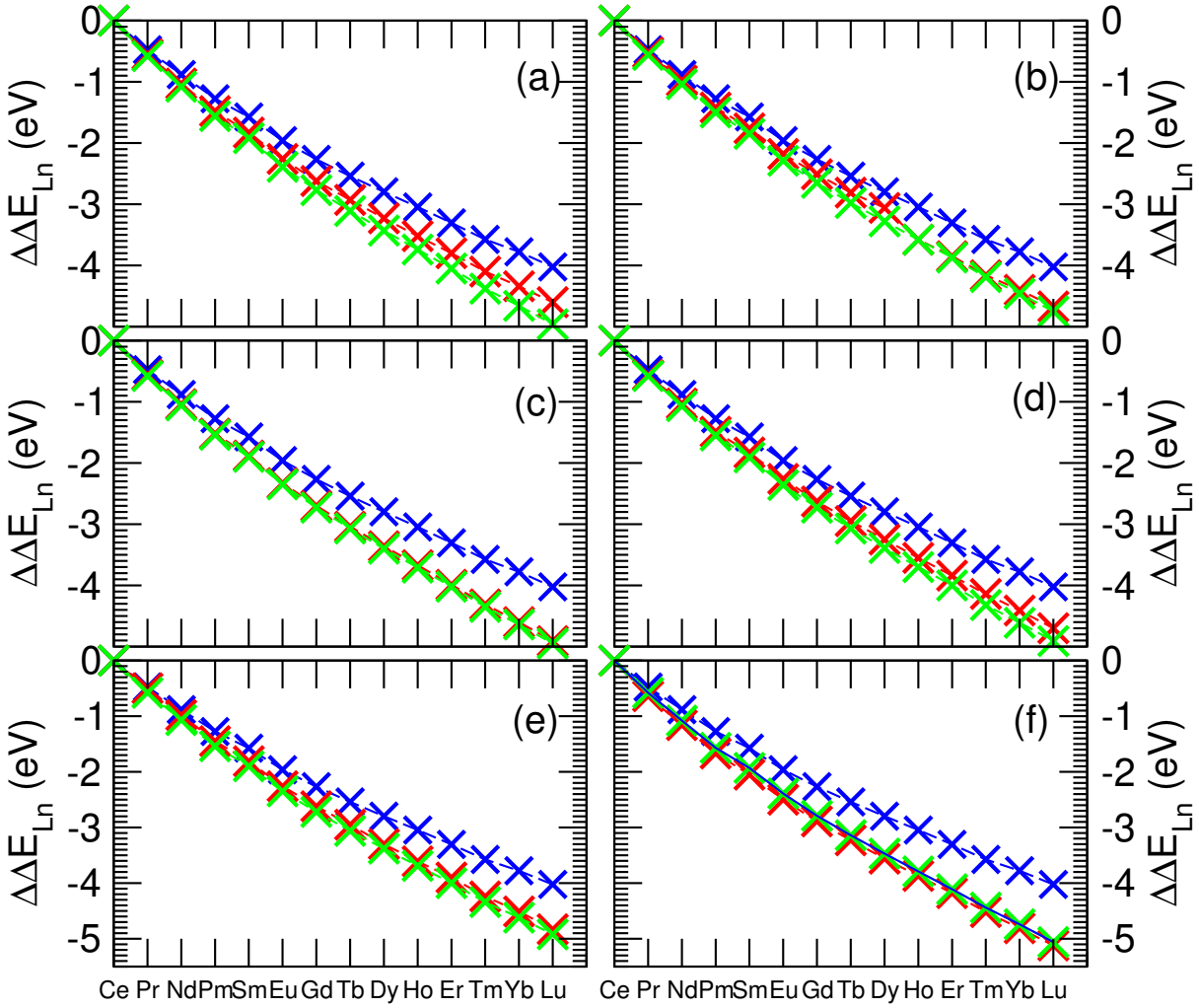

FIG. 7: $\Delta\Delta E$ across 14 Ln^{3+} relative to Ce^{3+}. Panels (a)-(f) correspond to those in Fig. 6. Red and green denote configurations generated using the Ce^{3+} and Lu^{3+} trajectories, respectively. Blue depicts Ln^{3+} coordinated to 8 water molecules.

The monotonic energy increase as the Ln^{3+} radius decreases is consistent with the trend predicted for some organic macrocycles in the literature.[21] Our $\Delta\Delta\Delta E$ is also up to ~3 times larger in magnitude than that in Ref. 21. Unlike those cases, the uncertainty and variability of ligand speciation, local surface site density, and location of anchor sites mean that the conclusions from our model studies will be qualitative rather than quantitative. Also of note

is the prediction that the mixed ligand system of Fig. 7d, with a PYC and an oxalate, does not yield cooperative advantage, i.e., $\Delta\Delta E$ which is qualitatively different from those with two oxalates (Fig. 7c).

In most cases the Ce- and Lu-configurations feature the same number of H_2O molecules and their total energies can be directly compared; the Lu-configurations are found to be more energetically favorable in total energies. Even with the weak PYC ligand, the lighter Ln^{3+} is not favored, unlike for PYC in Fig. 5. The main reason appears that the other strong ligands for Ln^{3+}, like the oxalate and SiO^- groups, which strongly favors the heavier Ln^{3+}, overcome the slight PYC preference for lighter Ln^{3+}. This trend is likely due to a combination of direct coulomb interactions, polarization, and induction effects. Dispersion forces does not strongly influence the trend (ESI Sec. S1).

Finally, we consider a binding site with an unmistakably "repulsive" ligand to examine whether the inference gleaned from the PYC calculation in Fig. 5, namely that repulsive ligands may favor lighter Ln^{3+}, can be implemented on β-cristobalite surfaces. We replace the N-atom in the PYC in Fig. 6d with a C-H group, which should repel Ln^{3+}. After optimizing the atomic configuration, the modified PYC becomes displaced from the Ln^{3+} (Fig. 9b). Even though the Ln^{3+} now has a lower coordination number than with PYC, the $\Delta\Delta E$ across the Ln^{3+} remains strongly favorable to the heavier Ln^{3+} compared to 8 water molecules in the Ln^{3+} solvation shell. We hypothesize that a rigidly structured binding site, with a combination of weak and strong ligands to Ln^{3+}, may be needed to select lighter or intermediate-radius Ln^{3+} from heavier ones from a mixture in aqueous solutions.

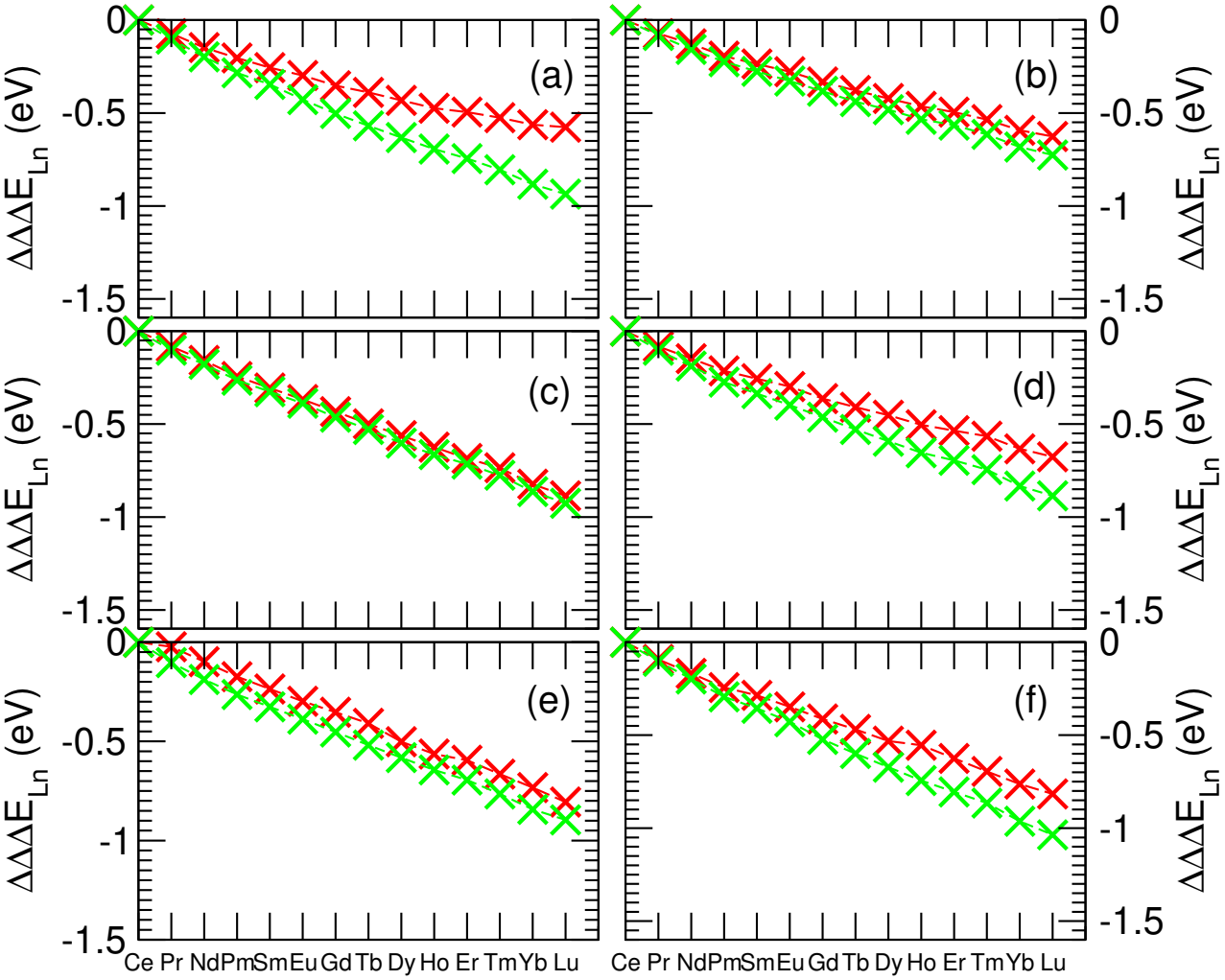

FIG. 8: $\Delta\Delta E$ across 14 Ln^{3+} for the ligands corresponding to Fig. 6(a)-(f) after subtracting the $\Delta\Delta E$ in water. Red and green denote configurations generated using the Ce^{3+} and Lu^{3+} trajectories, respectively.

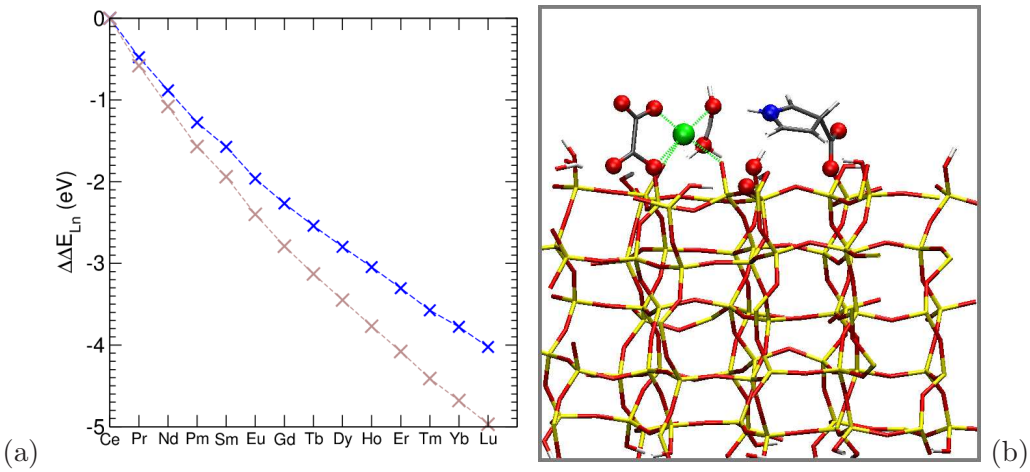

FIG. 9: (a) $\Delta\Delta E$ across 14 Ln^{3+} for the ligands (beige) corresponding to the structure in Fig. 9(b). This structure corresponds to Fig. 6d, but with a CH group replacing an N-atom on the aromatic ring. See Fig. 6 for the color key. In panel (a), the blue line is for Ln^{3+} coordinated to 8 water molecules.

IV. CONCLUSIONS

We have applied two types of calculations to examine the differential adsorption free energies ($\Delta\Delta G$) or differential binding enegies ($\Delta\Delta E$) of Ln^{3+} at a binding site in aqueous media, referenced to either that of a neighboring Ln^{3+} in the periodic table, or to Ce^{3+}. Perturbative AIMD simulations show that two simple ionic ligands like sulfates, phosphates, and mixed sulfate-and-phosphate favors the heavier/smaller Dy^{3+} than its lighter/larger neighbor Tb^{3+} by 0.30-0.31 eV. The mixed sulfate/phosphate system does not exhibit unusual cooperative binding interactions. A similar value is obtained at a UiO-66 binding site. In water, that difference is 0.29 eV. The 0.01-0.02 eV difference, between water and water-plus-ligands, is a fraction of the thermal energy, and should lead to observable preference for Dy^{3+} at room temperature, provided that the cancellation of DFT uncertainties in the AIMD correlated sampling calculations is sufficient. The primary amine $C_2H_5NH_2$ yields a $C_2H_5NH_3^+/OH^-/Ln^{3+}$ motif at the binding site, but the binding free energy is weak, and this ligand is not expected to directly bind to Ln^{3+} in water.

Perturbative AIMD is rigorous when the trajectories are sufficiently long, but are computationally costly. To obtain $\Delta\Delta E$ trends for 14 lanthanides bracketed by Ce and Lu at binding sites consisting of two ligands tethered to β-cristobalite surfaces, we use a more cost-efficient approach that involves short AIMD runs to supply the local coordination structure and then configuration optimization to calculate the total energies. While not guaranteed to attain the global energy minimum, the qualitative trends when switching between different Ln^{3+} within the same optimized binding site should be relevant. The ligands involved are aspartate, oxylate, mixed aspartate/oxalate, NP_3, and bare, deprotonated silica surfaces, all of which has locally negatively charged head groups. In all cases, the $\Delta\Delta E$ slope as the Ln^{3+} radius decreases is steeper than $\Delta\Delta E$ with 8 water molecules, meaning that the heavier Ln^{3+}'s are favored. Lu^{3+} prefers to bind to the negatively charged ligand-binding sites than to water by as much as 1.1 eV over Ce^{3+}. This suggests strong Ln^{3+} selectivity from the aqueous media.

This brings us back to the possible role of mixed ligands and cooperative binding. If our goal is to design binding sites that preferentially adsorb the lighter Ln^{3+} from water over the heavier ones, one option is to use weak, even partially positively-charged ligands that destabilize the adsorption of heavy Ln^{3+}. However, sites with lower binding free energies compared with Ln^{3+} hydration free energy would cause the Ln^{3+} to stay in water and

not adsorb. The pairing of strong, negatively charged ligand, with a weak, even repulsive ligand, may then be an approach that can preferentially select lighter Ln^{3+}, provided that the binding site is sufficiently rigid that repulsive ligands cannot diffuse away from the Ln^{3+}. This will be the subject of future studies. Ln^{3+} concentration and entropy effects will also be considered in the future.

Acknowledgement

We thank Boyoung Song, Eric Sikma, Dorina Sava-Gallis, Jacob Harvey, and Louise Criscenti for useful input. This work was supported by the Laboratory Directed Research and Development Program at Sandia National Laboratories (project # 225932). This article has been authored by an employee of National Technology & Engineering Solutions of Sandia, LLC under Contract No. DE-NA0003525 with the U.S. Department of Energy (DOE). The employee owns all right, title and interest in and to the article and is solely responsible for its contents. The United States Government retains and the publisher, by accepting the article for publication, acknowledges that the United States Government retains a non-exclusive, paid-up, irrevocable, world-wide license to publish or reproduce the published form of this article or allow others to do so, for United States Government purposes. The DOE will provide public access to these results of federally sponsored research in accordance with the DOE Public Access Plan https://www.energy.gov/downloads/doe-public-access-plan. This paper describes objective technical results and analysis. Any subjective views or opinions that might be expressed in the paper do not necessarily represent the views of the U.S. Department of Energy or the United States Government.

---

[1] J.H.L. Voncken, *The Rare Earth Elements: An Introduction.* (Springer, 2015).

[2] N. Krishnamurthy, C.K. Gupta, *Extractive Metallurgy of Rare Earths.* (2016, CRC press)

[3] G. Ferru, D.G. Rodrigues, L. Berthon, O. Diat, P. Bauduin and P. Guilbaud, *Angew. Chem. Int. Ed.* 2014, **53**, 5346-5350.

[4] I. Lehman-Andino, J. Su, K.E. Papathanasiou, T.M. Eaton, J.W. Jian, D. Dan, T.E. Albrecht-Schmitt, C.J. Dares, E.R. Batista, P. Yang, J.K. Gibson, K. Kavallieratos, *Chem. Commun.* 2019, **55**, 2441-2444.

[5] F.W. Lewis, L.M. Harwood, M.J. Hudson, A. Geist, V.N. Kozhevnikov, P. Distler, J. John, *Chem. Sci.* 2015, **6**, 4812-4821.

[6] H.J. Zhang, R.G. McDowell, L.R. Martin, Y. Qiang, *ACS Appl. Mater. Interfaces* 2016, *8*, 9523-9531.

[7] Y. Peng, H. Huang, Y. Zhang, C. Kang, S. Chen, L. Song, D. Lui, C. Zhong. *Nat. Commun.* 2018, **9**, 187.

[8] S.-L. Yeh, D. Alexander, N. Narasimhalu, R. Koshani, A. Sheikhi. *ACS Appl. Mater. Interfaces* 2023, **15**, 44154-44166.

[9] C. Falaise, C. Volkringer, R. Giovine, B. Prelot, M. Huve, T. Loiseau. *Dalton Trans.* 2017, **46**, 12010.

[10] V. Balos, B.A. Marekha, C. Malm, M. Wagner, Y. Nagata, M. Bonn, *et al. Angew. Chemie Int. Ed.* 2019 **58**, 332-337.

[11] A. Valverde, G.I. Tovar, N.A. Rio-Lopez, D. Torres, M. Rosales, S. Wuttke, A. Fidalgo-Marijuan, J.M. Porro, M. Jimenez-Ruiz, V.G. Sakai, A. Garcia, J.M. Laza, J.L. Vilas-Vilela, L. Lezama, M.I. Arriortua, G.J. Copello, R.F. de Luis. *Chem. Mater.* 2022, **34**, 96669684

[12] A. Hu, S.N. MacMillan, J.J. Wilson. *J. Am. Chem. Soc.* 2020, **142**, 13500-13506.

[13] R.E. Sikma, B. Song, J.I. Deneff, J.Smith, K. Sanchez, R.A. Reyes, E.T. Nguyen, L.M. Lureco, A.G. Ilgen, D.F. Sava-Gallis. *Chem. Commun.* 2024, https://doi.org/10.1039/D4CC00320A

[14] A.S. Ivanov and V.S. Bryantsev, *Eur. J. Inorg. Chem.* 2016, **21**, 3474-3479

[15] M.R. Healy, A.S. Ivanov, Y. Karslyan, V.S. Bryantsev, B.A. Moyer and S. Jansone-Popova, *Chem. Eur. J.* 2019, **25**, 6326-6331.

[16] B. Sadhu and M. Dolg, *Inorg. Chem.* 2019, **58**, 9738-9748.

[17] J. Ciupka, X. Cao-Dolg, J. Wiebke and M. Dolg, *Phys. Chem. Chem. Phys.* 2010, **12**, 13215-13223.

[18] C. Boehme, G. Wipff. *Chem. Eur. J.* 2001, **7**, 1398-1407.

[19] Y.A. Ustynyuk, M.Y. Alyapyshev, V.A. Babain, N.A. Ustynyuk. *Rus. Chem. Rev.* 2016, **85**, 917-942.

[20] T. Liu, K.R. Johnson, S. Jansone-Popova, D. Jiang. *JACS Au* 2022, **2**, 1428-1434.

[21] T. Liu, A.S. Ivanov, I. Popovs, S. Jansone-Popova, D. Jiang. *RSC Adv.* 2023, **13**, 764.

[22] T. Vercouter, B. Amekraz, C. Moulin, E. Giffaut, P. Vitorge. *Inorg. Chem.* 2005 **44**, 7570-7581.

[23] P.E. Reiller, T. Vercouter, L. Duro, C. Ekberg. *Appl. Geochem.* 2011, **27**, 414-426.

[24] A.I. Mishustin. *Rus. J. Inorg. Chem.* 2012, **57**, 712-716.

[25] R.H. Byrne, J.H. Lee, L.S. Bingler. Rare Earth Element Complexation by PO_4^{3-} Ions in Aqueous Solution. *Geochim. et Cosmochim. Acta* 1991, **55**, 2729-2735.

[26] P. Paoletti. *Pure & Appl. Chem.* 1984, **56**, 491-522.

[27] C. de Stefano, O. Giuffre, S. Sammartano. *J. Chem. Eng. Data* 2005, **50**, 1917-1923.

[28] P. D'Angelo, A. Zitolo, V. Migliorati, G. Chillemi, M. Duvail, P. Vitorge, S. Abadie and R. Spezia, *Inorg. Chem.* 2011, **50**, 4572-4579.

[29] P. D'Angelo and R. Spezia, *Eur. J. Chem.* 2012 **18**, 11162-11178.

[30] V. Migliorati, A. Serva, F.M. Terenzio and P. D'Angelo, *Inorg. Chem.* 2017, **56**, 6214-6224.

[31] I. Persson, P. D'Angelo, S. De Panfilis, M. Sandström and L. Eriksson, *Chem. Eur. J.* 2008, **14**, 3056-3066.

[32] V. Migliorati, A. Serva, F. Sessa, A. Lapi, P. D'Angelo. *J. Phys. Chem. B* 2018, **122**, 2779-2791.

[33] J. Kuta, M.C.F. Wander, Z. Wang, S. Jiang, N.A. Wall, A.E. Clark. *J. Phys. Chem. C* 2011, **115**, 21120-21127.

[34] J. Kuta and A.E. Clark, *Inorg. Chem.* 2010, **49**, 7808-7817.

[35] D. Yu, R. Du, J.-C. Xiao, S. Xu, C. Rong and S. Liu, *J. Phys. Chem. A* 2018, **122**, 700-707.

[36] R.S. Dybczyński, K. Kulisa, M. Pyszynska, A. Boganowska-Czajka. *J. Chromatography A* 2015, **1386**, 74-80.

[37] D.S. Jordan, J.N. Malin and F.M. Geiger, *Environ. Sci. Technol.* 2010, **44**, 5862-5867.

[38] D.S. Jordan, S.A. Saslow and F.M. Geiger, *J. Phys. Chem. A* 2011, **115**, 14438-14445.

[39] D. Garcia, J. Lützenkirchen, V. Petrov, M. Siebentritt, D. Schild, G. Lefevre, T. Rabung, M. Altmaier, S. Kalmykov, L. Duro and H. Geckeis, *Coll. Surfaces A* 2019, **578**, 123610.

[40] A.G. Ilgen A.G. Non-provisional patent application "Systems and Methods for Separating Rare Earth Elements Using Mesoporous Materials." Filed on 3/11/2020.

[41] Y. Hu, E. Drouin, D. Lariviere, F. Kleitz and F.-G. Fontaine, *ACS Appl. Mater. Interfaces* 2017, **9**, 38584-38593.

[42] S. Giret, Y. Hu, N. Masoumifard, J.-F. Boulanger, E. Juere, F. Kleitz and D. Lariviere, *ACS Appl. Mater. Interfaces*, 2018, **10**, 448-457.

[43] A. Li, H. Zhai, J. Li, Q. He, *Chem. Lett.* 2020, *49*, 1125-1135.

[44] N. Krishnamurthy, C.K. Gupta, *Extractive Metallurgy of Rare Earths, 2nd Edition* (CRC Press, 2015)

[45] J.E. Sutton, S. Roy, A.U. Chowdhury, L. Wu, A.K. Wanhala, N. De Silva, S. Jansone-Popova, B.P. Hay, M.C. Cheshire, T.L. Windus, A.G. Stack, A. Navrotsky, B.A. Moyer, B. Doughty, V.S. Bryantsev. *ACS Appl. Mater. Interfaces*, 2020, **12**, 16327-16341.

[46] R.C. Chapleski, A.U. Chowdhury, A.K. Wanhala, V. Bocharova, S. Roy, P.C. Keller, D. Everly, S. Jansone-Popova, A. Kisliuk, R.L. Sacci, A.G. Stack, C.G. Anderson, B. Doughty, V.S. Bryantsev. *iScience*, 2020, **23**, 101435.

[47] R.C. Chapleski, A.U. Chowdhury, A.K. Wanhala, L.D. Gibson, D. Stamberga, S. Jansone-Popova, R.L. Sacci, H.M. Meyer, A.G. Stack, V. Bocharova, B. Doughty, V.S. Bryantsev. *Langmuir*, 2022, **38**, 5439-5453.

[48] J.A. Cotruvo *ACS Central Sci.* 2019, **5**, 1496-1506.

[49] Y. Liu, Y. Chen, Y. *Acc. Chem. Res.* 2006, **39**, 681-691.

[50] M.N. Regueiro-Figueroa, K. Djanashvili, D. Esteban-Gomez, T. Chauvin, E. Toth, A. de Blas, T. Rodriguez-Blas, C. Platas-Iglesias. *Inorg. Chem.* 2010, **49**, 4212-4223.

[51] O. Alptürk, O. Rusin, S.O. Fakayode, W. Wang, J.O. Escobedo, I.M. Warner, W.E. Crowe, V. Král, J.M. Pruet, R.M. Strongin, *Proc. Nat. Acad. Sci.* 2006, **103**, 9756-9760.

[52] R. Poirot, X. Le Goff, O. Diat, D. Bourgeois, D. Meyer. *ChemPhysChem* 2016, **17**, 2112-2117.

[53] H.H. Dam, D.N. Reinhoudt, W. Verboom. *Chem. Soc. Rev.* 2007, **36**, 367-377.

[54] A. Karmakar, M. Duvail, M. Bley, T. Zemb, J.-F. Dufreche. *Coll. Sur. A* 2018, **555**, 713-727.

[55] S.H. Hewitt, G. Macey, R. Mailhot, M.R. Elsegood, F. Duarte, A.M. Kenwright, S.J. Butler. *Chem. Sci.* 2020, **11**, 3619-3628.

[56] R.J. Ellis, Y. Meridiano, R. Chiarizia, L. Berthon, J. Muller, L. Couston, M.R. Antonio. *Chem. Euro. J.* 2013, **19**, 2663-2675.

[57] P.W. Huang. *ChemistrySelect* 2019, **4**, 12368-12374.

[58] J.A. Peters, K. Djanashvili, C.F. Geraldes, C. Platas-Iglesias, *Coord. Chem. Rev.* 2020, **406**, 213146.

[59] I. Fryer-Kanssen, J. Austin, A. Kerridge. *Inorg. Chem.* 2016, **55** 10034-10042.

[60] N.A. Thiele, J.J. Woods, J.J. Wilson, *Inorg. Chem.* 2019, **58**, 10483-10500.

[61] R.J. Ellis, D.M. Brigham, L. Delmau, A.S. Ivanov, N.J. Williams, M.N. Vo, B. Reinhart, B.A. Moyer, V.S. Bryantsev. *Inorg. Chem.* 2017, **56**, 1152-1160.

[62] T.S. Grimes, C.R. Heathman, S. Jansone-Popova, A.S. Ivanov, S. Roy, V.S. Bryantsev, P.R. Zalupski. *Inorg. Chem.* 2018, **57**, 1373-1385.

[63] L. Troxler, A. Dedieu, F. Hutschka, G. Wipff, *J. Mol. Structure: THEOCHEM* 1998, **431**, 151-163.

[64] J.-H. Lan, W.-Q. Shi, L.-Y. Yuan, J. Li, Y.-L. Zhao, Z.-F. Chai, *Coord. Chem. Rev.* 2012, **256**, 1406-1417.

[65] Z. Wang, N. Pu, Y. Tian, C. Xu, F. Wang, Y. Liu, L. Zhang, J. Chen, S. Ding. *Inorg. Chem.* 2018, **58**, 5457-5467.

[66] R.D. Hancock, L.J. Bartolotti. *Inorg. Chim. Acta* 2013, **396**, 101-107.

[67] Y.-M. Chen, C.-Z. Wang, Q.-Y. Wu, J.-H. Lan, Z.-F. Chai, C.-M. Nie, W.-Q. Shi, *J. Mol. Liquids* 2020, **299**, 112174.

[68] X.-H. Kong, Q.-Y. Wu, C.-Z. Wang, J.-H. Lan, Z.-F. Chai, C.-M. Nie, W.-Q. Shi. *J. Phys. Chem. A* 2018, **122**, 4499-4507.

[69] S. Umetani, Y. Kawase, Q.T. Le, M. Matsui. *Inorg. Chim. Acta* 1998, **267**, 201-207.

[70] D.J. Vogel, D.F. Sava-Gallis, T.M. Nenoff, J.M. Rimsza. *Phys. Chem. Chem. Phys.* 2019, **21**, 23085-23093.

[71] V.P. Solov'ev, Y.A. Ustynyuk, N.I. Zhokhova, K.V. Karpov. *Mol. Informatics* 2018, **37**, 1800025.

[72] Gaussian 09, Revision A.1, M.J. Fritsch, *et al.*, Gaussian, Inc., Wallingford CT, 2009.

[73] R. Atta-Fynn, E.J. Bylaska, W.A. de Jong, *J. Phys. Chem. Lett.* **2013**, *4*, 2166-2170.

[74] K. Leung, A.G. Ilgen, L.J. Criscenti, *Phys. Chem. Chem. Phys.* 2021, **23**, 5750.

[75] R.C. Shiery and D.C. Cantu, *J. Phys. Chem. C* 2023, **127**, 4218.

[76] R.C. Shiery, J.L. Fulton, M. Balasubramanian, M.-T. Nguyen, J.-B. Lu, J. Li, R. Rousseau, V.-A. Glezakou, D.C. Cantu. *Inorg. Chem.* 2021, **60**, 3117-3130.

[77] D.M. Driscoll, R.C. Shiery, M. Balasubramanian, J.L. Fulton, D.C. Cantu. *Inorg. Chem.* 2022, **61**, 287-294.

[78] H.-S. Kim, *Chem. Phys.* 2001, **269**, 295-302.

[79] K. Leung, L.J. Criscenti, A.W. Knight, A.G. Ilgen, T.A. Ho, J.A. Greathouse. *J. Phys. Chem. Lett.* 2018, **9**, 5379-5385.

[80] A.W. Knight, P. Ilani-Kashkouli, J.A. Harvey, J.A. Greathouse, T.A. Ho, N. Kabengi, A.G. Ilgen. *Environmental Science: Nano* 2020, **7**, 68-80.

[81] J.P. Perdew, K. Burke, and M. Ernzerhof, *Phys. Rev. Lett.* 1996, **77**, 3865-3868.

[82] G. Kresse, and J. Furthmüller, *Phys. Rev. B* 1996, **54**, 11169-11186.

[83] G. Kresse, J. Furthmüller, *Comput. Mater. Sci.* 1996, **6**, 15-50.

[84] G. Kresse and D. Joubert, *Phys. Rev. B* 1999, **59**, 1758-1775.

[85] J. Paier, M. Marsman and G. Kresse, *J. Chem. Phys.* 2007, **127**, 024103.

[86] See, e.g., S. Grimme, *J. Comput. Chem.*, 2006, **27**, 1787-1799.

[87] V. Kostal, P.E. Mason, H. Matinez-Seara and P. Jungwirth, *J. Phys. Chem. Lett.* 2023, **14**, 4403.

[88] G. Hummer, L.R. Pratt, A. Garcia, *J. Chem. Phys.* 1997, **107**, 9275-9277.

[89] M.G. Martin and A.P. Thompson, *Fluid Phase Equil.* 2004, **217**, 105-110.

[90] K. Leung, I.M.B. Nielsen and L.J. Criscenti, *J. Am. Chem. Soc.*, 2009, **131**, 18358-18365.

[91] H.J.C. Berendsen, J.R. Grigera and T.P. Straatsma, *J. Phys. Chem.* 1987, **91**, 6269-6271.

[92] R.T. Cygan, J.-J. Liang, and A.G., Kalinichev *J. Phys. Chem. B* **108**, 1255, (2004).

[93] T. Leung, S.B. Rempe, O.A. von Lilienfeld. *J. Chem. Phys.* 2009, **130**, 204507.

[94] D. Jiao, K. Leung, S.B. Rempe and T.M. Nenoff, *J. Chem. Theory Comput.* 2011, **7**, 485.

[95] T.R. Graham, M. Dembowski, E. Martinez-Baez, X. Zhang, *et al.*, *Inorg. Chem.* 2018, **57**, 11864-11873.

[96] M. Pouvreau, M. Dembowski, S.B. Clark, J.G. Reynolds, K.M. Rosso, G.K. Schenter, C.I. Pearce, A.E. Clark, *J. Phys. Chem. B* 2018, **122**, 7394-7402.

[97] W. Zhang, R.Q. Honaker. *Int. J. Coal Geology* 2018, **195**, 189-199.